A wind farm consisting of two turbines - The combined influence of turbine spacing and rotational direction

Journal of Physics: Conference Series **2767** (2024) 092070 doi:10.1088/1742-6596/2767/9/092070

A wind farm consisting of two turbines - The combined influence of turbine spacing and rotational direction

Antonia Englberger[1], Andreas Dörnbrack[1]

[1]Institut für Physik der Atmosphäre, DLR Oberpfaffenhofen, Germany

E-mail: antonia.englberger@dlr.de

Abstract. Large-eddy simulations are conducted to investigate the impact of an actual decrease in turbine spacing on the wake structure for a small wind park consisting of two wind turbines in a row with a given rotor diameter D. A systematic variation of the inflow conditions (near-neutral and veering inflow) and the rotational direction of the rotors (clockwise and counterclockwise) provides an initial overview of the atmospheric flow fields in the wakes of both turbines. Whereas a smaller turbine spacing under near-neutral conditions results in a decrease of the streamwise flow component and an increase of turbulence, the situation is much more complicated under veering inflow. If a clockwise (counterclockwise) rotating turbine interacts with a Northern Hemispheric Ekman spiral, the combination of a rotor-induced v-component, which reduces (slightly amplifies) the meridional inflow velocity component, leads to a weakening (slight intensification) of this meridional wind in the vicinity of the downwind rotor.

1. Introduction

When old rotors of wind turbines are replaced with new ones, the efficiency and the size of the turbines is typically increased. However, with larger rotors being installed at the same distances (smaller relative turbine spacing Δ_{WT} with respect to the new rotor diameter D) by using the grounding of the old wind turbines, the loads on the downwind blades will be affected. The associated change of the wake flow needs to be considered in the design process.

The loading and also the produced power of a wind farm strongly depend on the prevailing atmospheric flow regime. Assuming idealized conditions without mesoscale impacts, a neutral stratified flow is represented by a near-surface gradient of the streamwise wind, which approaches to zero at the height of the rotor. In stably-stratified situations, the streamwise and the lateral wind components are characterized by strong vertical gradients, resulting in a wind-direction change with height. This Ekman spiral results from the interaction between the Coriolis force and surface friction. In addition to the mean profiles, the turbulent fluctuations in both atmospheric flow regimes differ, with higher fluctuations in the neutral case, whereas the stable case is characterized by less turbulent kinetic energy due to buoyant destruction in the vertical. Both inflow wind properties are interacting with the wind-turbine rotor, resulting in a stretching of the wake from a circular shape in neutral cases to an ellipsoid under stable conditions [1, 2]. Further, the difference in the turbulent kinetic energy continues in the wake, with lower values in stably-stratified regimes [2].

Recent work of Englberger et al. [3] demonstrate the impact of the rotational direction on the wind-turbine wake in stably-stratified inflow, which results from the interaction of the vertical change of the wind-direction and the spanwise velocity component imposed by the rotor on the atmosphere. This study reveals an impact of the rotational direction of the rotor on both the wake width and the deflection angle. Further, Chanprasert et al. [4] performed wind-park simulations for the southern hemisphere (negative Coriolis parameter and consequently a reversed Ekman spiral), resulting in an impact of the wake shape twist angle. These results state a rotational direction impact in wind parks, which could be suitable for wind park control. Our work uses the rotational direction of the rotor as an additional free parameter. This approach is reasonable, as the interaction of a common clockwise rotating rotor with a Northern Hemispheric Ekman spiral shows the same characteristic wake patterns as the interaction of a counterclockwise rotating rotor operating in a Southern Hemispheric Ekman spiral [5]. In the context of a wind-park, Englberger et al. [6] showed a power and loading increase of the downwind turbine in case of a counterclockwise rotating upfront rotor. The study was performed for a turbine spacing of 7 D, which is often used in LES [2]. The general turbine spacing in wind farms range from $3\,D$ to $10\,D$ [7]. Recent research wind-park configurations result in a narrower turbine spacing, e.g. $4.5\,D$ in WiValdi [8]. Therefore, this study reduces the previously used spacing of $7\,D$ [6] down to $3\,D$. for a wind-park arrangement with two wind turbines in a row with a given rotor diameter D. The rotational direction is used as additional free parameter to study the interaction of both, the spanwise atmospheric wind component and the rotor-induced flow. The paper is organized as follows: The numerical model, the wind park configuration, the prevailing atmospheric conditions and a simulation overview is given in Sect. 2. The impact of turbine spacing on the streamwise velocity and turbulent kinetic energy (TKE) and on the spanwise and vertical velocity components in the wakes follows in Sect. 3 and Sect. 4. Conclusions are given in Sect. 5.

2. Objectives and Methodology

2.1. The numerical model

In the large-eddy simulation (LES), the Boussinesq equations for incompressible atmospheric flow are solved for the Cartesian velocity components u, v, and w and for the potential temperature perturbation $\Theta^{'} = \Theta - \Theta_e$, with the background state Θ_e, following [9, 10].

$$\frac{d\mathbf{v}}{dt} = -\boldsymbol{\nabla}\left(\frac{p^{'}}{\rho_0}\right) + \mathbf{g}\frac{\Theta^{'}}{\Theta_0} - 2\,\Omega_C\,(\mathbf{v} - \mathbf{v}_e) + \beta\frac{\mathbf{F}_{WT}}{\rho_0} + \boldsymbol{\mathcal{V}}, \tag{1}$$

$$\frac{d\Theta^{'}}{dt} = -\mathbf{v}\nabla\Theta_e + \mathcal{H}, \tag{2}$$

$$\boldsymbol{\nabla}\cdot(\rho_0\mathbf{v}) = 0. \tag{3}$$

The atmosphere is dry with a constant density $\rho_0 = 1.1\,\mathrm{kg\ m^{-3}}$ and a constant reference value $\Theta_0 = 300$ K. In Eqs. (1), (2) and (3), $p^{'}$ represents the pressure perturbation with respect to the background state, $\mathbf{g}$ the vector of acceleration due to gravity, Ω_C the angular velocity vector of the Earth's rotation, and $\mathbf{F}_{WT}$ the turbine-induced forces on the atmospheric flow. The axial and tangential forces of the wind turbine, acting on the atmospheric flow, are parameterized with the actuator disc method. The prefactor β can be set to $\beta = +1$ in case of a common clockwise rotating rotor (CR) and to $\beta =$ -1 representing a counterclockwise rotating rotor (CCR). $\boldsymbol{\mathcal{V}}$ and $\boldsymbol{\mathcal{H}}$ are the viscous dissipation of momentum and heat, representing the subgrid-

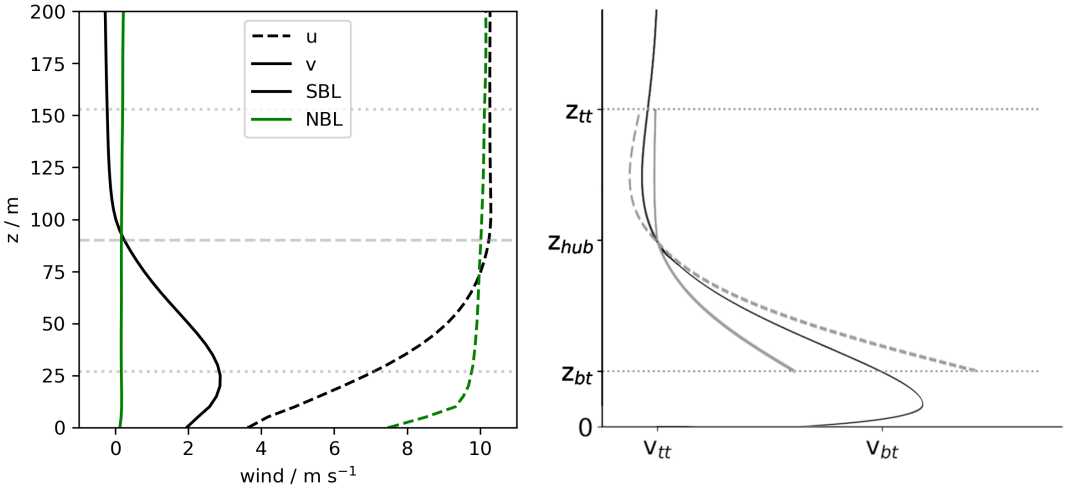

Figure 1: The vertical profiles of the atmospheric precursor simulation representing the NBL and the SBL in for the zonal velocity u and the meridional velocity v. The schematic illustration on the right represents the v-component of the SBL and the impact of a clockwise rotating rotor (solid gray lines) and a counterclockwise rotating rotor (dashed gray lines) on v. The horizontal lines represent the NREL 5 MW wind turbine, with top tip (tt) and bottom tip (bt).

scale (SGS) contribution of turbulence. As SGS model, the TKE closure following Schumann [11] is applied. All simulations are performed with free-slip (partial-slip) boundary conditions at the top (bottom) of the domain. Further, EULAG uses Neumann boundary conditions to prescribe the SGS fluxes of momentum and heat.

2.2. Atmospheric conditions

Two different atmospheric conditions of a neutral boundary layer (NBL) and a stable boundary layer (SBL) are considered in this study. Both atmospheric flow fields result from a diurnal cycle simulation. For a more detailed description of this diurnal cycle simulation we refer to Englberger and Dörnbrack [12].

The mean values of the zonal (u - west-east) and meridional (v - north-south) wind components in Fig. 1 show an important difference between the NBL and the SBL flow regimes. Whereas the NBL flow has no vertical gradient of the meridional component, $\frac{dv}{dz}$ is non-zero in the SBL case, which is an effect of surface cooling and the Coriolis force. Further, the vertical gradient of the zonal wind component $\frac{du}{dz}$ is also much larger during the night. Therefore, the nocturnal mean flow is characterized by a wind direction change with height, affecting the lower half of the rotor, whereas in case of near-neutral stratification, the inflow wind is perpendicular to the rotor at each height. The cooling of the surface during night further reduces the turbulent kinetic energy in SBL in comparison to NBL [12][Fig. 2 b and d]. In the Northern (Southern) Hemisphere, a veering $\frac{dv}{dz} > 0$ (backing $\frac{dv}{dz} < 0$) wind is the effect of the Coriolis force, occurring in approximately 75% of measured events [13, 14].

The average wind shear exponent between 60 m and 140 m height calculated from the overall observational dataset at the WiValdi wind farm is 0.25 and during night $\alpha = 0.31$ [15]. In the idealized SBL case considered here for the NREL 5 MW rotor, $\alpha(\text{rotor}) = 0.24$ and $\alpha(\text{lower rotor half}) = 0.35$. Therefore, the wind shear exponent in the SBL is comparable to the observations, while the height of the boundary layer is a free parameter.

2.3. Wind-park conditions

In this study, we consider a wind farm arrangement consisting of two turbines, one in the wake of the other. This arrangement is similar to the current OPUS 1 and 2 installation at the research wind park WiValdi [8]. As wind turbines, we apply the 5 MW NREL wind turbine with a rotor diameter $D = 126$ m and a hub height of 90 m. The hub height is very similar to OPUS 1 and 2 of 92 m. Their rotor diameters are 116 m which is slightly smaller than that of the NREL rotor. However, the turbine data of OPUS 1 and 2 were not yet available at the time we performed this study.

The wind-park simulations are performed with a synchronized coupling with the precursor atmospheric simulation by applying 2 D slices of u, v, w and Θ as inflow condition at each time step. For more details we refer to [12][Sect. 2.3]. All wind-park simulations are performed with an equidistant horizontal grid spacing of 5 m on 1024 x 512 grid points and a grid spacing increase from 5 m to 10 m in the vertical. The 130 m thick damping layer starts at 300 m.

2.4. Simulation overview

This study systematically investigates the interaction of three factors by means of LESs:

- atmospheric stratification (near-neutral and stable stratification),
- wind-turbine spacing ($\Delta_{WT} \in [3\ D; 7\ D]$ in $1\,D$ steps),
- rotational direction (four combinations of rotational direction in SBL case).

In the following investigations, averages of the last 10 min of the corresponding wind-farm simulation are denoted by $\overline{(\ldots)}$ and are applied to calculate the streamwise velocity $\overline{u_{i,j,k}}$, the velocity deficit $VD_{i,j,k} \equiv \frac{\overline{u_{1,j,k}} - \overline{u_{i,j,k}}}{\overline{u_{1,j,k}}}$, and the turbulence kinetic energy $TKE_{i,j,k} = 0.5(\overline{u'^2_{i,j,k}} + \overline{v'^2_{i,j,k}} + \overline{w'^2_{i,j,k}})$, with primed quantities defined as differences between the local values at the grid point (i, j, k) and their temporal averages, respectively.

3. The turbine-spacing impact on streamwise velocity and TKE

This study compares the impact of repowering on the wakes of both wind turbines for neutral and stably-stratified regimes, with a special emphasis on the stable case. Therefore, the wake structure at 60 m (lower rotor half) of the two wind turbines is presented in Figure 2 for a spacing of $3\,D$ in the first row, increasing to a spacing of $7\,D$ in the last row. The left column represents the two clockwise rotating wind turbines in the NBL, the middle column represents the same wind-turbine setup under stably-stratified inflow conditions, and the right column represents two counterclockwise rotating wind turbines operating in the SBL.

The impact of the prevailing meridional wind component (Fig. 1) can clearly be seen by comparing the first column with $v = 0$ for the NBL to the both right columns with $v > 0$ for the SBL. A persistent meridional flow component during night leads to a deflection of the wake of both wind turbines. This feature has been investigated in previous studies [1, 2, 12].

A new focus of this study is the impact of turbine spacing on the boundary-layer flow of the downwind turbine. In case of near-neutral inflow, a shorter distance changes the operation conditions of the second wind turbine in such a way that lower flow velocities (higher VD) interact with the downwind rotor. Behind the downwind rotor, VD is inversely proportional to the turbine spacing, i.e. it becomes smaller for larger Δ_{WT}. This inverse proportionality is similar for both rotational directions of the rotors in the stably-stratified case, with one exception. Approaching to very small turbine spacings, the upwind wake incorporates the wake of the downwind turbine associated with higher values of VD in comparison to a larger ($\Delta_{WT} \geq 5\,D$) turbine spacing.

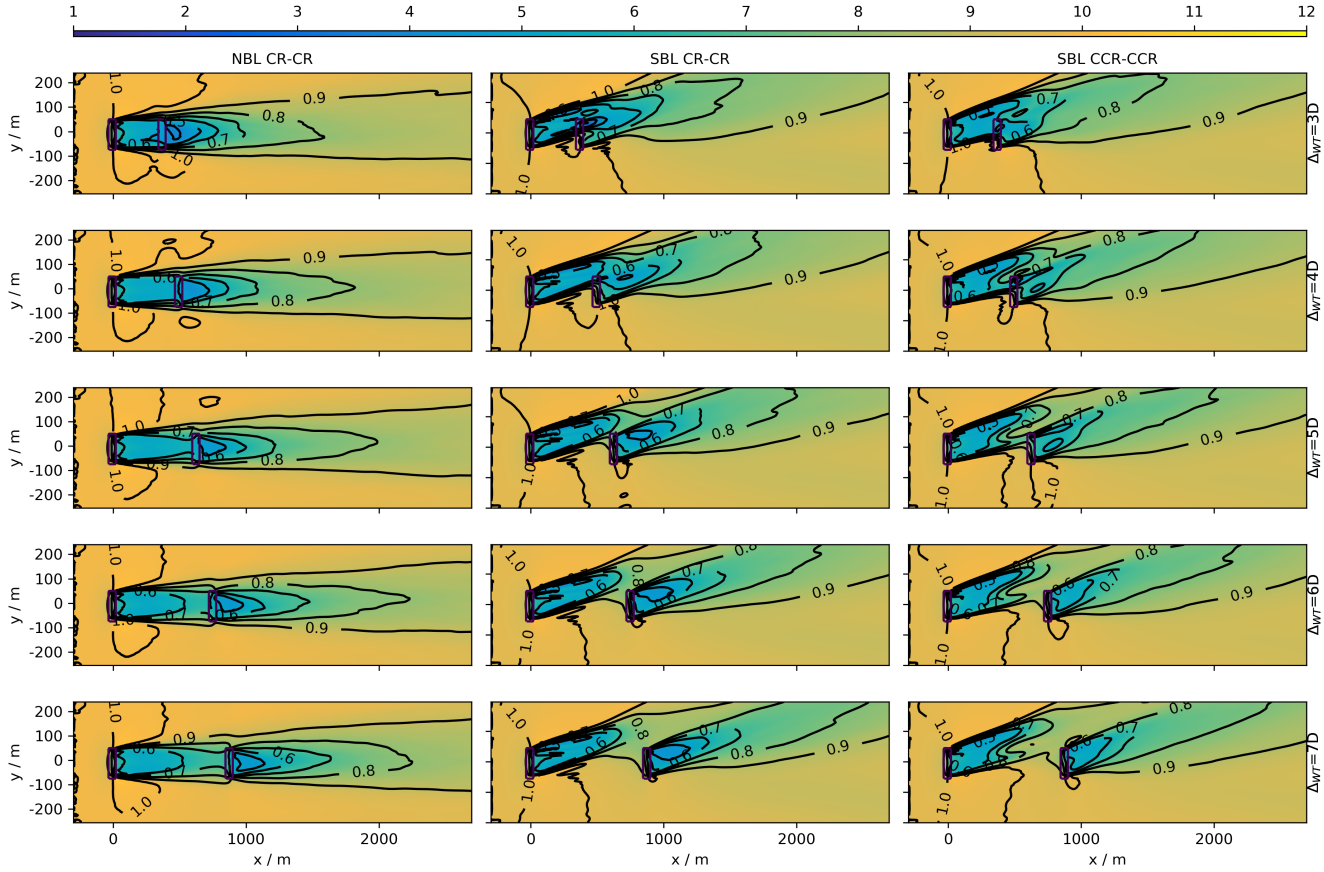

Figure 2: Coloured contours are the averaged streamwise velocity component u (m s^{-1}) in the lower half of the rotor. Black contours denote the velocity deficit VD. The corresponding atmospheric situation and rotational direction of the rotors are marked at the top of each column and the turbine spacings can be found on the right.

A more detailed investigation of the impact of turbine spacing on the atmosphere for all possible combinations of rotational directions under veering inflow is presented in Figure 3. The drop-off magnitude of the rotor-averaged flow component $\Delta\overline{u_{A_r}}$ at the corresponding downwind position for $\Delta_{WT} \leq 5\,D$ depends on the turbine-spacing for the NBL. A larger Δ_{WT} results in a very similar minimum value of $\overline{u_{A_r}}$. The streamwise evolution plot for all stable cases shows a similar behaviour. The shorter Δ_{WT}, the smaller $\Delta\overline{u_{A_r}}$ at the downwind rotor, whereas $\Delta\overline{u_{A_r}}$ starts to level out at the same value for $\Delta_{WT} \geq 5\,D$. This different behaviour for $\Delta_{WT} \leq 5\,D$ results from smaller values of $\overline{u_{A_r}}$ in front of the downwind rotor. The slightly larger $\overline{u_{A_r}}$ values in comparison to the neutral stratification result from the typical ellipsoidal wake structure under nocturnal inflow conditions, which results from the vertical gradient of the spanwise velocity component.

These findings are summarized in Fig. 4. Each rectangle represents the rotor and time averaged value $\overline{u_{A_r}}$ of Fig. 3. The values of $\overline{u_{A_r}}$ are calculated at discrete positions every 1 D in x - direction. All cases show a decrease of $\overline{u_{A_r}}$ if Δ_{WT} decreases.

The right column of Fig. 3 represents the rotor area averaged TKE. In case of neutral atmospheric flow (NBL CR-CR case), $\overline{TKE_{A_r}}$ as well as the maximum of $\Delta\overline{TKE_{A_r}}$ increase if Δ_{WT} decreases. In case of veering inflow, the pattern is similar, with a decrease of $\overline{TKE_{A_r}}$ for

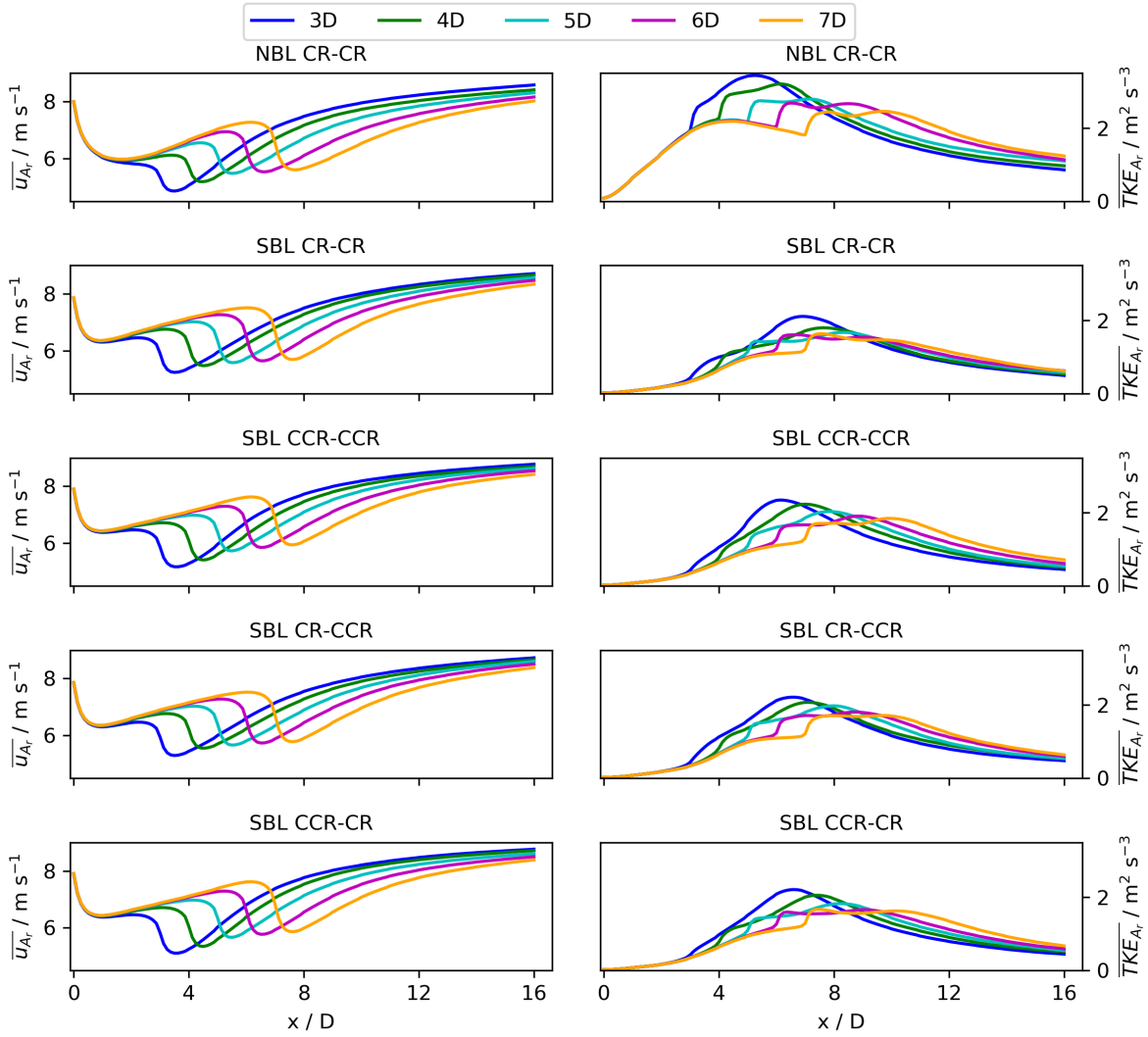

Figure 3: Rotor area and time averaged values $\overline{u_{A_r}}$ (left column) and $\overline{TKE_{A_r}}$ (right column) in dependence of the distance from the first wind turbine. Each line represent a different combination of atmospheric inflow and rotational direction of the turbines.

larger Δ_{WT}. Further, if a counterclockwise rotating rotor is involved, the maximum of $\overline{TKE_{A_r}}$ is reached at a smaller downwind distance.

4. The turbine-spacing impact on spanwise and vertical velocity

The main impact of the rotational direction is the sign of the spanwise component v the rotor imposes on the atmosphere. The inflow wind field results from a precursor simulation, where the inflow streamwise wind is from the west to the east ($u > 0$) (Fig. 1). The spanwise component of the atmosphere is under veering inflow from south to north ($v > 0$). In case of a clockwise rotating rotor, the flow component of the rotor imposed on the wake is counterclockwise, i.e.

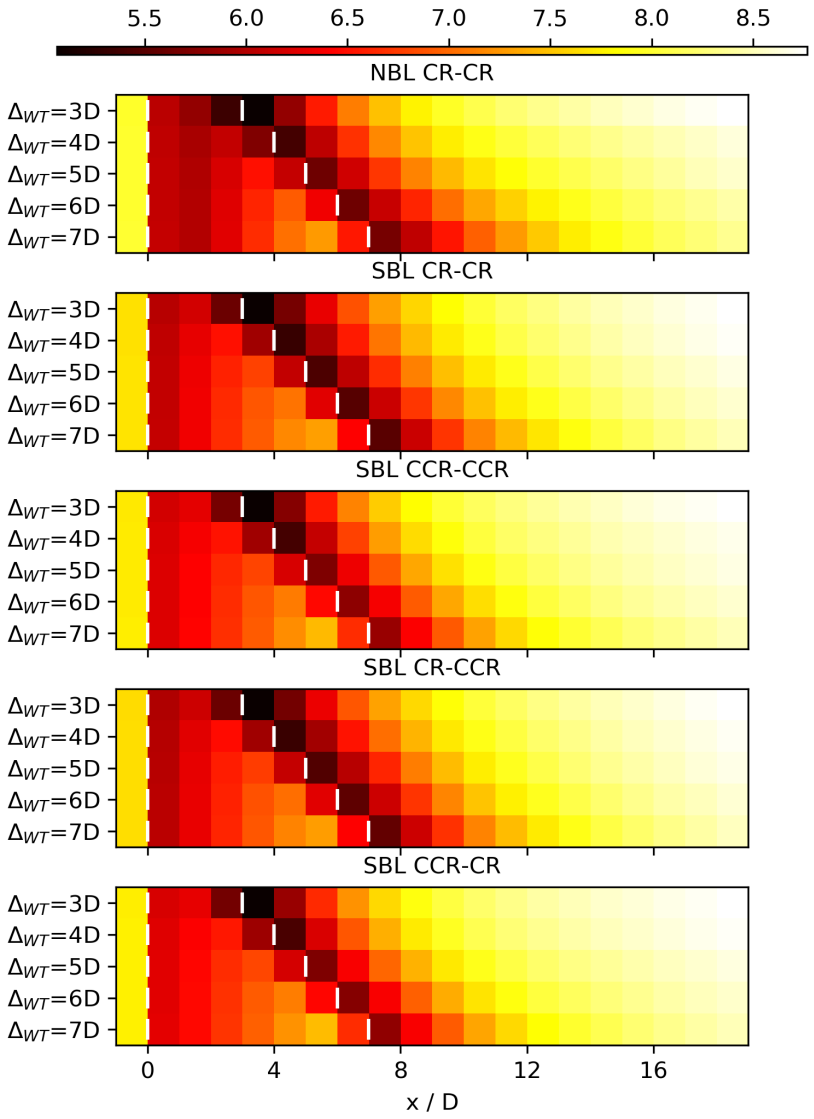

Figure 4: Rotor area and time averaged values $\overline{u_{A_r}}$ (left column of Fig. 3) for every rotor diameter on the x-axis. The y-axis represents the corresponding wind-turbine spacing Δ_{WT}. The white vertical lines represent the position of the wind turbines.

from north to south in the lower rotor half. In this case both v-components of the ABL and the rotor are opposed to each other, which leads to a massive change in v as schematically illustrated by the gray solid line in Fig. 1. In case of a counterclockwise rotating rotor, the rotor-induced v-component is from south to north, reinforcing the inflow v-component like in the dashed gray curve of Fig. 1 [3].

Figure 5 represents the v-component of the wake in the left column, which is the superposition of the atmospheric component with the rotor-induced component. The NBL CR-CR case

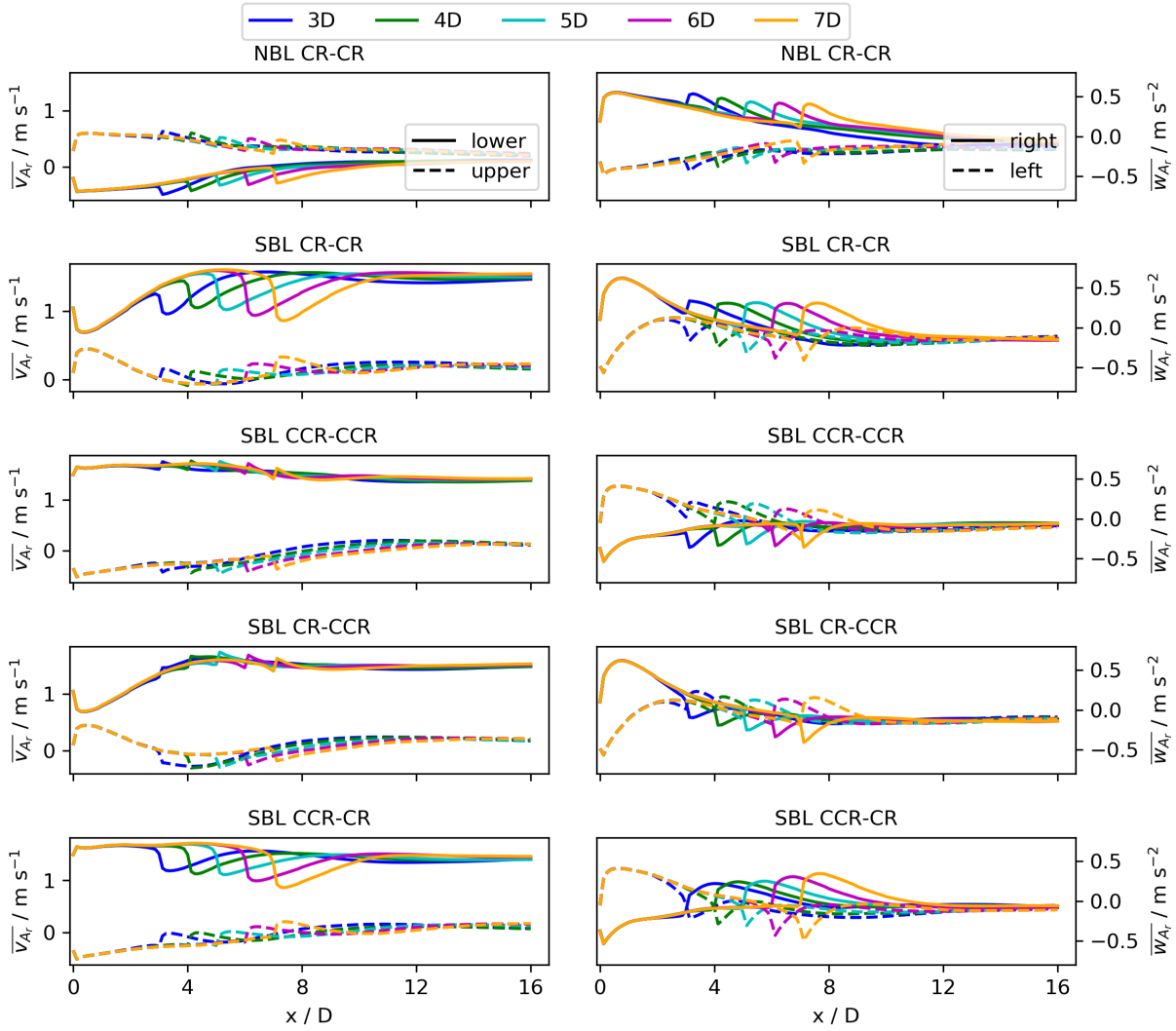

Figure 5: Same as in Fig. 3, only for the v-component on the left and the w-component on the right. Here, the values of $\overline{v_{A_r}}$ ($\overline{w_{A_r}}$) are averaged over the lower and the upper (right and left) rotor half separately.

represents only the contribution of the rotor as in the inflow $v = 0$, with $v > 0$ in the upper rotor half and $v < 0$ in the lower rotor part. The v-component is stronger for smaller Δ_{WT} spacings, as the rotation of the flow field behind the first rotor is superposed and intensified by the rotation of the second one. If Δ_{WT} increases, the rotation of the first rotor is fading out, leading to smaller $\Delta\overline{v_{A_r}}$-values at the position of the downwind rotor. The situation is similar for SBL CCR-CCR, only the absolute v-values are larger in the lower rotor half in comparison to the upper rotor half, which is related to the atmospheric Ekman spiral and the atmospheric v-component of 1.5 m s^{-1} at this height (Fig. 1). Further, the maxima in v_{lower} and v_{upper} differs in the sign in comparison to NBL CR-CR, as the rotational direction of the rotors is the opposite.

In SBL CR-CR, the resulting $\overline{v_{A_r}}$ component has a smaller magnitude at the position of the first wind turbine, since the v-components from the atmosphere and the rotor are directed in opposite directions, which leads to an attenuation of $\overline{v_{A_r}}$ behind the first turbine. The same process is repeated at the position of the second turbine, which in turn leads to a further weakening of $\overline{v_{A_r}}$ in the wake of the downwind rotor. Here, $\Delta\overline{v_{A_r}}$ at the specific turbine location is larger in the lower rotor half, which is consistent with the neutral case, whereas $\Delta\overline{v_{A_r}}$ is very similar in both rotor halves in the SBL CCR-CCR case. Further, $\Delta\overline{v_{A_r}}$ increases for a larger turbine spacing Δ_{WT}.

In the right column of Fig. 5, the vertical velocity component w of the atmosphere is presented for the right and the left rotor half (looking from west towards the rotor disc). The behaviour of $\overline{w_{A_r}}$ corresponds to the expectation resulting from the rotational direction of the rotor. In case of a clockwise (counterclockwise) rotating rotor, the $\overline{w_{A_r}}$-component is positive (negative) in the right, southern half and negative (positive) in the left, northern half. The cases NBL CR-CR and SBL CCR-CCR show a constant value of $\Delta\overline{w_{A_r}}$ for all turbine spacings Δ_{WT}, which is in agreement with the behaviour of the v-component. However, for the combination of veering inflow and two clockwise rotating rotors, the value of $\Delta\overline{w_{A_r}}$ increase for larger turbine spacings Δ_{WT}.

A more detailed picture results from the investigation of a combination of a clockwise and a counterclockwise rotational direction for both wind turbines. For the CR-CCR case, the plots of the v- and the w-components are very similar to the corresponding ones for two counterclockwise rotating rotors (CCR-CCR case). The rotational combination CCR-CR, however, shows as similar picture as the CR-CR case.

5. Conclusion

As the importance of a decrease in turbine spacing (e.g. repowering) will increase in the near future, this study is a first investigation of the effects of turbine spacing on the atmospheric flow field in a sequence of LESs. The rotational direction of the rotor is used as an adjustable parameter to identify the impact of the interaction of the inflow v-component with the rotor-induced v-component on the atmospheric flow field in the wake.

The general assumption of a decrease of the streamwise flow component and an increase of TKE for decreasing turbine distances and their interaction with the downwind rotor is certainly valid under near-neutral inflow. For a veering inflow, the situation is more complicated, as the meridional flow component of the atmosphere plays a crucial role. Of special interest is the superposition of the two v-components of the atmosphere and the rotor with opposite signs, which leads to a weakening of the v-w-flow field in the very near wake of the downwind rotor.

Further investigations are required to determine whether this finding can be used to maximize the power generated by a wind farm. In this work, only one characteristic northern hemisphere nighttime atmospheric regime is presented. But the basic physical processes are supposed to be consistent. The question is to what extend the magnitude of the three impact parameters, the atmospheric stratification, the turbine spacing, and the rotational direction, modifies the described interaction.

The understanding of the exact physical processes occurring for narrower turbine spacing is especially interesting for the research wind farm WiValdi, as the physical distance between the two turbines is 508 m, resulting in a turbine spacing of 4.4 D and also the wind shear exponent of this idealised study is applicable to WiValdi.

Acknowledgements

The authors gratefully acknowledge the Gauss Centre for Supercomputing e.V. (https://www.gauss-centre.eu) for funding this project by providing computing time on the GCS Supercomputer SuperMUC at Leibniz Supercomputing Centre (LRZ, https://www.lrz.de).

References

[1] Vollmer, L., Steinfeld, G., Heinemann, D. and Kühn, M. 2016 Estimating the wake deflection downstream of a wind turbine in different atmospheric stabilities: an LES study *Wind Energy Sci* **1**(2), 129-141.
[2] Abkar, M. and Portè-Agel, F. 2016 The effect of atmospheric stability on wind-turbine wakes: A large-eddy simulation study *J. Phys. Conf. Ser.* **27(3)**
[3] Englberger, A., Dörnbrack, A. and Lundquist, J. K. 2020 Does the rotational direction of a wind turbine impact the wake in a stably stratified atmospheric boundary layer? *Wind Energy Sci* **5**(4), 1359-1374.
[4] Chanprasert, W., Sharma, R. N., Cater, J. E. and Norris, S. E. 2022 Large Eddy Simulation of wind turbine wake interaction in directionally sheared inflows. *Renewable Energy* **201**, 1096-1110.
[5] Englberger, A., Lundquist, J. K. and Dörnbrack, A. 2020 Changing the rotational direction of a wind turbine under veering inflow: A parameter study *Wind Energy Science* **5**
[6] Englberger, A., Wrba, L., Dörnbrack, A. and Lundquist, J. K. 2022 How does the rotational direction of an upwind turbine affect its downwind neighbour? *J. Phys. Conf. Ser.* **2265**(2)
[7] Porté-Agel, F., Bastankhah, M., and Shamsoddin, S. 2020 Wind-turbine and wind-farm flows: A review. *Boundary-Layer Meteorology* **174.1**, 1-59.
[8] https://windenergy-researchfarm.com
[9] Smolarkiewicz, P. K., Sharman, R., Weil, J., Perry, S. G., Heist, D. and Bowker, G. 2007 Building resolving large-eddy simulations and comparison with wind tunnel experiments *J Comput. Phys* **227**, 633-653.
[10] Prusa, J. M., Smolarkiewicz, P. K. and Wyszogrodzki, A. A. 2008 EULAG, a computational model for multiscale flows *Comput. Fluids* **37**, 1193-1207.
[11] Schumann, U. 1991 Subgrid length-scales for large-eddy simulation of stratified turbulence *Theoretical and Computational Fluid Dynamics* **2(5-6)**
[12] Englberger, A. and Dörnbrack, A 2018 Impact of the diurnal cycle of the atmospheric boundary layer on wind-turbine wakes: a numerical modelling study *Boundary-Layer Meteorology* **166**, 423-448.
[13] Walter, K., Weiss, C. C., Swift, A. H., Chapman, J. and Kelley, N. D. 2009 Speed and direction shear in the stable nocturnal boundary layer *J. Sol. Energ.-T.* **131**
[14] Sanchez Gomez, M. and Lundquist, J. K. 2020 The effect of wind direction shear on turbine performance in a wind farm in central Iowa *Wind Energy Science* **5**, 125-139.
[15] Wildmann, N., Hagen, M. and Gerz, T. 2022 Enhanced resource assessment and atmospheric monitoring of the research wind farm WiValdi *J. Phys. Conf. Ser.* **2265**